

# Quantitative Nanofriction Characterization of Corrugated Surfaces by Atomic Force Microscopy\*

A. Podestà, G. Fantoni,<sup>†</sup> and P. Milani<sup>‡</sup>

*INFN - Dipartimento di Fisica, Università degli Studi di Milano,  
Via Celoria 16, 20133 Milano, Italy*

(Dated: November 9, 2018)

## Abstract

Atomic Force Microscopy (AFM) is a suitable tool to perform tribological characterization of materials down to the nanometer scale. An important aspect in nanofriction measurements of corrugated samples is the local tilt of the surface, which affects the lateral force maps acquired with the AFM. This is one of the most important problems of state-of-the-art nanotribology, making difficult a reliable and quantitative characterization of real corrugated surfaces. A correction of topographic spurious contributions to lateral force maps is thus needed for corrugated samples. In this paper we present a general approach to the topographic correction of AFM lateral force maps and we apply it in the case of multi-asperity adhesive contact. We describe a complete protocol for the quantitative characterization of the frictional properties of corrugated systems in the presence of surface adhesion using the AFM.

---

\*Submitted to Journal of Applied Physics, Feb. 2003

<sup>†</sup>Present address: Agusta, Lab. Tecnol. Materiali - Controlli Non Distruttivi - via G. Agusta, 520 Cascina Costa di Samarate (VA), Italy

<sup>‡</sup>Electronic address: pmilani@mi.infn.it

## I. INTRODUCTION

The study of tribological properties at sub-micrometer scales has been stimulated by the reduction of dimensions of mechanical devices. Micro Electro-Mechanical Systems (MEMS), Nano Electro-Mechanical Systems (NEMS), or hard disk drives require an accurate control of friction, wear, and adhesion at the nanometer scale [1, 2, 3]. From a fundamental point of view the investigation of the influence of the chemico-physical condition of the surface at the nanoscale on the tribological behavior can provide important elements for the understanding of friction, wear, and lubrication phenomena.

Atomic Force Microscopy (AFM) is one of the most powerful techniques for the investigation of tribology and in particular of nano-friction [4, 5, 6]. An atomic force microscope can simultaneously acquire topographic maps of surfaces with nanometric resolution, and friction maps operating in the so-called Friction-Force mode. Friction Force Microscopy (FFM) is possible thanks to the simultaneous acquisition of the vertical deflections of the beam supporting the AFM tip, related to changes in the topographic relief, and the lateral deflections, proportional to the friction force between the tip and the sample surface [2, 7].

In order to perform quantitative friction measurements it is necessary to control and measure accurately the forces acting on the AFM tip. Parameters such as roughness, granularity, power spectrum of the surface play an important role. The effects of surface topography on nano-friction measurements have been studied, although a general theory is still lacking [8, 9, 10, 11, 12]. In many cases, attention has been concentrated on flat crystalline surfaces under ultra-high-vacuum (UHV), where the influence of surface topography is negligible [13, 14, 15, 16].

On the other hand, real surfaces in every-day conditions necessitate to take into account the topographic contribution to lateral force maps in order to achieve quantitative tribological information. Actually, in the case of corrugated samples, that is of locally tilted surfaces, the measured forces in the directions parallel and perpendicular to the AFM reference plane do not necessarily coincide with the forces acting parallel and perpendicularly to the sample surface, which actually define the friction coefficient and the friction vs. load characteristics of the interface under investigation [8, 9, 10, 11, 12]. These effects related to surface morphology depend on the ratio between the dimension of the sliding probe and that of the surface asperities. In this sense friction is a scale-dependent phenomenon, and a tool such

the AFM, which is able to provide morphological information on a wide range of scales, is very attractive for such studies.

In this paper we consider the role of the topographic correction in a general way and inquiry whether it is possible to follow a model-independent approach, providing the friction vs. load characteristics of the system under investigation without the need of postulating any particular contact-friction model. We discuss the experimental limitations, which make the model-independent approach unreliable and we solve the problem of the topographic correction in the particular case of the adhesive multi-asperity contact, which is of common occurrence in many experimental setups. To this purpose, we introduce a modified version of the Amonton's law for friction [17] (linear dependence of friction on the load), which should better apply to the case of low loads and few asperities in contact. We present our topographic correction procedure in the framework of a complete quantitative statistical protocol based on the AFM for the characterization of frictional properties of materials at sub-micron scale. We discuss the limit of validity of this model and highlight the underlying assumptions.

The article is organized as follows: in sections II and III we present the theory of the topographic correction of lateral force maps acquired with a standard beam deflection AFM; in section IV we discuss the multi-asperity adhesive contact regime typical of FFM experiments and present a friction model which should apply to FFM experiments in the presence of humidity; in section V we include this model in the topographic correction theory and derive the basic equations for interpreting the experimental data; in section VI we describe the experimental setup and the characterization protocol; in section VII we discuss the validity of the topographic correction protocol via its application to a corrugated Polytetrafluoroethylene surface. Conclusions are reported in section VIII.

## **II. FFM ON CORRUGATED SAMPLES: THE TOPOGRAPHIC CORRECTION**

In a typical FFM experiment the cantilever is scanned across the surface in a direction orthogonal to the long cantilever axis. Using a segmented photodiode, with two upper and two bottom quadrants, it is possible to measure accurately not only the vertical cantilever displacements, but also the cantilever lateral torsion. The vertical deflection of the cantilever is proportional to the applied load, while fluctuations around the average position are due

to corrugations of the sample surface [2]. These vertical fluctuations represent the input of a feedback loop, keeping the cantilever deflection, that is the applied load, constant. Recording the relative displacements of the tip-sample assembly provides the AFM topographic map. The torsion of the cantilever is in turn proportional to the friction force between the AFM tip and the sample surface. The acquisition of lateral cantilever deflections (the so-called lateral force signals) provides the friction map. Both topographic and friction maps can be recorded simultaneously. Fig. 1 shows a typical friction loop, i.e. the lateral force signals  $TR$  and  $RETR$  (in arbitrary units) acquired in the two opposite directions during a single scan (these directions are usually called Trace and Retrace). The typical loop shape is due to the fact that the lateral signal changes sign when the motion of the tip is reversed. The ramps at the beginning of the Trace and Retrace curves are due to a *pivot* effect during the reversal of the tip motion.

In order to achieve a quantitative understanding of the friction properties of a surface one needs to consider closely the contact regime occurring during the experiment. Contact regimes in FFM and standard macroscopic friction tests can be very different [18, 19]. In typical FFM measurements, the radius of curvature of the AFM tip can be comparable or even smaller to the size of morphological surface features (few nanometers). If  $\xi$  is a measure of the average extension of morphological features of the surface (the correlation length of the surface can be used [20]) and  $R$  is the AFM tip radius, the aforementioned situation is characterized by the condition  $\xi/R \geq 1$  (Fig. 2, right). In this case a single-asperity contact is to be expected [21]. The limiting case is represented by a sharp spherical or parabolic tip (as those prepared via electron beam deposition techniques [22]) sliding on an atomically smooth surface (a situation which can be well realized in UHV-FFM apparatus). In macroscopic friction experiments a slider, typically a ball or a disk, is scanned across a surface with a geometric or apparent contact area as large as few  $cm^2$  [19]. As long as the dimension of the slider is large compared to  $\xi$  ( $\xi/R \leq 1$ , Fig. 2, left), a multi-asperity contact is to be expected [21].

The friction coefficient  $\mu$  is defined as the ratio  $f/N$ , where  $f$  is the opposing friction force acting on the slider in the direction perpendicular to the local surface normal and  $N$  is the load applied along the surface normal. The presence of a global tilt of the surface, that is a tilt on a scale comparable or larger than that of the probe, can affect the measurement of the friction coefficient. This is because in typical friction apparatus the forces tangential

and perpendicular to the ideally flat laboratory reference plane are measured, say  $T$  and  $L$ . If the surface is tilted,  $T$  and  $L$  are no longer parallel to  $f$  and  $N$ , accordingly. A topographic correction to the measured quantities  $T$  and  $L$  is thus necessary in order to get the values of  $f$  and  $N$  and from these the value of the friction coefficient [8, 9, 10, 11, 12]. In many experimental situations, typically in macroscopic friction tests, the sample surface is supposed to be flat on a length scale large compared to the slider dimension. In this case the measured forces corresponds to the local normal and tangential components, and the above definition of the friction coefficient readily applies. In FFM experiments on corrugated surfaces however the probe is likely to be scanned on a locally tilted surface, as shown in Fig. 2. The topographic correction is thus an essential part of any protocol devoted to the quantitative characterization of frictional properties of surfaces.

A good parameter characterizing the flatness of the sample surface is the local slope  $\tan(\theta)_R$ . The pedex  $R$  means that the slope is calculated with resolution equal to the slider dimension. For the surface to be considered locally tilted, it is necessary that the tilt extends on a length bigger than the slider dimension (i.e.  $\tan(\theta)_R \neq 0$ ), as shown in Fig. 2, where the local tilt of the surface,  $\theta^*$ , is calculated with resolution equal to the radius of the bigger probe. The map of local slopes is readily obtained from the topographic map. Because of the possibility of acquiring simultaneously the topographic and the lateral force maps, FFM is the technique of choice to perform accurate friction measurements at those small scales where the topographic correction is required.

In order to consider the topographic correction, we show in Fig. 3 the forces acting on the AFM tip sliding over a sloped surface. The negative sign indicates the retrace direction. Notice that  $\theta \equiv \theta_R$  is the local surface tilt. The tip is forced against the object by two forces exerted by the cantilever: one is the applied load  $\mathbf{L}$ [43], directed downward, the other is the tangential force  $\mathbf{T}$  originating in the torsion of the cantilever, in the direction of motion. Three other forces act on the tip: the friction force  $\mathbf{f}$ , perpendicular to the local normal and always opposing the motion, the local surface adhesion  $\mathbf{A}$ , directed as the local normal, and a normal reaction  $\mathbf{\Phi}$ , equal in magnitude but opposite in direction to the *total* applied load  $\mathbf{N}$ . It should be noticed that while the applied load  $\mathbf{L}$ , the adhesion force  $\mathbf{A}$  and the surface reaction  $\mathbf{\Phi}$  have always the same direction, the tangential and friction forces  $\mathbf{T}$  and  $\mathbf{f}$  invert their direction as the motion is reversed, from Trace to Retrace.

Projecting the equilibrium condition  $\mathbf{T} + \mathbf{f} + \mathbf{L} + \mathbf{\Phi} + \mathbf{A} = \mathbf{0}$  for Trace (+) and Retrace

(-) along the local normal and tangential axes provides a system of four equations, which represents the topographic correction, providing  $f$  and  $N$  as a function of  $T$ ,  $L$ ,  $A$  and  $\theta$ :

$$\begin{aligned}
f_+ &= T_+ \cos(\theta) - L \sin(\theta) \\
N_+ &= L \cos(\theta) + T_+ \sin(\theta) + A \\
f_- &= T_- \cos(\theta) + L \sin(\theta) \\
N_- &= L \cos(\theta) - T_- \sin(\theta) + A
\end{aligned} \tag{1}$$

Given a number of  $(f, N)$  pairs, the model-independent friction vs. load curve of the interface considered is obtained. Depending on the mechanics of the contact (single or multi-asperity), both a power law and a linear behavior can be observed [21]. Interesting physical parameters such as the friction coefficient, the surface energy, the true contact area etc. can in principle be extracted fitting the experimental  $f$  vs.  $N$  curve.

In the above equations  $T$  is the force acting parallel to the AFM reference plane. In fact, what is measured are the true lateral force signals,  $T_{\pm}$ , plus an instrumental offset  $T_{instr}$  ( $TR$  and  $RETR$ , which form the friction loop shown in Fig. 1). Assuming the instrumental offset to be independent on the direction of motion, we have:

$$\begin{aligned}
TR &= T_+ + T_{instr} \\
RETR &= -T_- + T_{instr}
\end{aligned} \tag{2}$$

We can now reconsider more closely the friction loop in Fig. 1 in order to express the equations of the topographic correction in terms of measurable quantities. A vertical offset  $\Delta$  is present in the friction loop, causing the loop having a non-zero average. The offset  $\Delta$  of the friction loop is calculated as:

$$\Delta = 1/2 \cdot (TR + RETR) \tag{3}$$

Also indicated in Fig. 1 is the average half width of the loop,  $W$ :

$$W = 1/2 \cdot (TR - RETR) \tag{4}$$

Substituting Eqs. 2 into Eqs. 3 and 4 we obtain:

$$\begin{aligned}
W &= \frac{T_+ + T_-}{2} \\
\Delta &= T_{instr} + \frac{T_+ - T_-}{2}
\end{aligned} \tag{5}$$

We see from Eqs. 5 that even if we were able to subtract point-by-point the instrumental offset from the friction loop, still the loop average would be non-zero, but equal to  $(T_+ + T_-)/2$ . This residual offset is intrinsically due to the presence of a local non-zero slope, causing the local effective load  $N$ , and consequently the local friction  $f$ , and the lateral signals  $T_+$  and  $T_-$  to be different in Trace and Retrace (see Eqs. 1). Moreover, it turns out that  $W$  is an approximation of both the Trace and Retrace lateral force signals  $T_+$  and  $T_-$ , i.e. an average lateral force. While the instrumental offset cancels out in Eq. 4 after the subtraction[44], there are spurious contributions to lateral force which do not cancel, having the same sign (but generally different magnitudes) in Trace and Retrace. These contributions are due to the *ploughing* and *collision* mechanisms reported for instance in Ref. 12. These spurious contributions are related to sudden changes in surface slope, but they can not be accounted for as we did for the other topographic contributions discussed above in that there is not any analytic relation to parameters such as slope, applied load and scanning velocity. However, provided the scanning velocity is not very high and the feedback loop of the AFM is properly adjusted, these spurious contributions to lateral force maps can be smoothed out if a large number of points in the map are acquired, in that they represent only a small fraction of the lateral force map.

Finally from Eqs. 5 we obtain:

$$\begin{aligned} T_+ &= W + \Delta - T_{instr} \\ T_- &= W - \Delta + T_{instr} \end{aligned} \tag{6}$$

Substituting Eqs. 6 into Eqs. 1, the model-independent friction characteristics  $f$  vs.  $N$  in terms of the measurable quantities  $W$  and  $D$  and the instrumental offset  $T_{instr}$  is obtained. In the following section we will discuss the properties of the instrumental offset and highlight the reasons why its measurement is not usually reliable.

### III. INSTRUMENTAL OFFSET

The instrumental offset  $T_{instr}$  is determined by thermal drifts of the cantilever, electronic noise, laser intensity fluctuations and laser interference, changes in the environmental conditions (temperature, relative humidity) and cross-talking effects, causing a spurious lateral signal even in the absence of any true lateral force. The instrumental offset can vary from

scan to scan, and also during the same scan, and it is in general load-dependent. Cross-talking represents the most important contribution to the instrumental offset [23, 24]. It is caused by a bad alignment of the laser beam with respect to the photodiode array. If the plane containing the beam is not perpendicular to the plane of the photodiodes, vertical displacements of the cantilever will cause a spurious lateral signal, even in the absence of any applied load and/or friction force. The alignment of the laser with respect to the cantilever and photodetector is thus a critical step in any FFM experiments. Some authors report about correction of the cross-talking effect via electronic compensation [24], however this imply the risk of manipulating the true signal and it is in general not simple to perform, in that it requires an accurate measurement of the spurious lateral force signal versus the applied load.

One way to characterize the instrumental offset is to record the lateral force signals during approaching-retracting cycles of the tip on the sample. Because the cantilever does not move laterally during approaching-retracting cycles, any lateral deflection measured by the photodiodes can be attributed to cross-talking effects. The force vs. distance curve and the lateral force curve are in one-by-one correspondence: the first provide the applied loads, while the second provides the spurious lateral force offset corresponding to each applied load. In Fig. 4 the  $T_{instr}$  vs. applied load curve acquired with the method described above is shown. The signals acquired in the approaching and retracting part of the cycle are different. Moreover, the spurious lateral force is not negligible, compared with typical frictional forces in FFM experiment (few nN). The presence of strong laser interference is visible.

It is definitely clear in Fig. 4 that the instrumental offset does depend in general on the applied load. This method is useful to qualitatively characterize the instrumental offset and its load dependence. However, it is not reliable. Even if one takes the average over many approaching-retracting cycles, the offset changes quickly, and the curve acquired before the FFM measurement is usually different from the one acquired after. Moreover, the bending and twisting of the cantilever during the approaching-retracting cycles does not mimic necessarily those occurring during the Trace and Retrace scans for any given applied load, if not qualitatively. In principle, a more reliable method to characterize quantitatively the instrumental offset could be to measure the spurious lateral deflections during free oscillations of the cantilever, at different oscillation amplitudes, which would correspond to different applied loads in contact mode. The drawbacks of this method, not implemented here, are



that only relatively small amplitudes can be set (i.e. low loads), and that the tip is not in contact with the sample, that is, there could be contact-induced contributions to the offset, which are not taken into account when measuring the free oscillations of the cantilevers.

The topographic correction (Eqs. 1 and Eqs. 6) based on the direct measurement of the instrumental offset is hampered by the difficulty in measuring reliably and accurately this essential parameter. A possible way to circumvent this problem is to fix, a priori, the friction regime (in fact, only the multi-asperity case can be worked out analytically, because of the simple linear dependence of friction on load). Apart from difficulties in the calculations, even for the simplest models, it must be pointed out that this strategy is not fully satisfactory, because it assumes the friction regime, while it would be better to infer it from experimental data. However, the validity of the model adopted can be confirmed, a posteriori, from the shape of the lateral force vs. load curves, and the choice of the model can be supported by reasonable assumptions about the material to be investigated and the size and shape of the AFM tip.

#### IV. ADHESION AND THE MODIFIED AMONTON'S LAW

In this section we address the problem of the adhesive contact between two surfaces, in order to define and possibly justify a reasonable friction model to be used in the equations of the topographic correction developed in the previous paragraphs.

A fundamental relation is the proportionality between the friction force  $f$  and the contact area  $a$  between two bodies [17]:

$$f = \tau a \tag{7}$$

$\tau$  being the shear modulus, i.e. the friction force per unit area. Eq. 7 has been verified experimentally both directly (with the Surface Force Apparatus [25] or friction-current measurements [26]) for single-asperity contacts and indirectly, through the validity of the contact mechanics models [15]. The shear modulus  $\tau$  depends in general on the number and nature of bonds forming at the interface, while the contact area depends on the mechanical properties of the interface, that is on the bulk properties of tip and sample materials.

Contact mechanics aims to provide for every contact regime the functional relation  $a(N)$  between the contact area  $a$  and the load  $N$ . Once the relation  $a(N)$  is established, the friction vs. load characteristics  $f(N)$  for a particular system is given by Eq. 7. Classical

contact mechanics for continuous elastic bodies was proved to be applicable to nanometer-sized contacts, as the ones occurring in FFM [13, 22, 26, 27].

FFM offers a wide spectrum of contact regimes, depending on both interface properties (tip radius, surface corrugation, as well as elastic properties of tip and sample), and environmental properties, such as relative humidity. The load range is also important in determining the contact regime. During FFM experiments on flat surfaces using well characterized spherical or parabolic tips a single-asperity contact is likely to take place [22]. When corrugated samples are investigated in ambient conditions, in the presence of humidity and contaminants, a multi-asperity contact is even possible, although the smoothing effect of contaminants of tip and sample nano-corrugations, leading to a transition from a multi- to a single-asperity contact, has also been observed [28]. The AFM allows indeed to investigate different contact regimes, provided a good characterization of the tip and sample morphology is given and the possibility of imaging under controlled environmental conditions.

In the case of non-adhering elastic and plastic multi-asperity contact, a linear dependence of friction on load  $L$  is expected, the so-called Amonton's law [17]:

$$f = \mu L \tag{8}$$

Given a load in the range [0-100] nN and a typical contact area from a few tens to a few thousands of nm<sup>2</sup>, a pressure in the MPa-GPa range is applied to the sample. This range is comparable to those of macroscopic friction tests, where loads are in the Newton range and contact areas can be up to few cm<sup>2</sup> [19]. However, in FFM, load can be comparable to adhesive forces (up to hundreds of nN). This implies that adhesion plays a fundamental role in every FFM experiment in ambient condition, and it is expected to strongly influence the friction behavior.

A considerable effort has been made in order to include adhesion in the models of multi-asperity elastic contact [29, 30, 31, 32, 33]. A definite model of roughness-dependent adhesion is still lacking. The available studies on adhesive multi-asperity contacts do not provide the relation between the area of contact and the load, which would provide in turn the actual friction law through Eq. 7 in the case of multi-asperity adhesive contacts. If adhesion is considered explicitly in Amonton's equations, setting  $N = L + A$ , where  $L$  is the external

applied load and  $A$  is the adhesion force, Eq. 8 becomes:

$$f = \mu N = \mu(L + A) \cong \text{const} + \mu L \quad (9)$$

This form of the Amonton's law is also known as the Coulomb equation [17]. At zero *external* applied load ( $L = 0$ ), Eq. 9 predicts a non-zero friction force, as in the case of both the Johnson-Kendall-Roberts (JKR) [34] and Derjaguin-Muller-Toporov (DMT) [35] models for the single-asperity adhesive contact. Unless the JKR model, however, the Coulomb law does not account for any finite frictional force in the limit of zero-total applied load, i.e. at pull-off. Another limitation of the Coulomb law is that adhesion  $A$  is considered constant, while it is reasonable that it varies with load, especially in the typical FFM conditions.

The contact mechanics of an FFM represents an intermediate case between the macroscopic multi-asperity case and the UHV single-asperity case, in that the contacting asperities, especially in the low-load regime, can be really a few. The SPM case lies in the low load, few asperities range where the asymptotic predictions of the different existing models fail. This point makes the study of the multi-asperity adhesive regime in FFM experiments very difficult. Without a complete contact theory, one may try to use reasonable models justifying them a posteriori with the experimental observations and theoretical results in the single-asperity limit. A possibility is to generalize Eq. 9 including an offset  $c$  in the linear dependence:

$$f^* \simeq \mu N + c \quad (10)$$

The linear dependence on load accounts for the fact that the contact is not single-asperity-like, especially when the AFM is operated on corrugated samples in humid air. The offset  $c$  accounts for the zero-total load friction force typical of many single-asperity contact, a limit not too far from the actual experimental situation. Moreover, as pointed out by Schwarz *et al.*, an offset in the Amonton's law accounts also for the uncertainty in the determination of the pull-off force [14, 36]. Whether the adhesive offset is due to uncertainty in the measurements of adhesion or is intrinsic, this can be proved a posteriori on the basis of its numerical value (see discussion below). Eq. 10 can be thought as the low-load limit of a more complex  $a \equiv a(N)$  dependence. The choice of a modified Amonton's law represents an attempt to generalize the Coulomb law in order to interpret friction data acquired with the FFM in common experimental situations, where a multi-asperity adhesive contact is likely to occur, but with only a few asperities in the low load regime.

## V. THE TOPOGRAPHIC CORRECTION FOR THE MODIFIED AMONTON'S LAW

We will consider Eq. 10 in the general framework of the topographic correction developed in Section II. We remind that in Eq. 10  $N$  represents the *total* applied load in the direction perpendicular to the surface, including the contribution of adhesion  $A$ . Substituting Eq. 10 in Eqs. 1 we obtain a new set of equations giving the values of  $T_+$ ,  $T_-$ ,  $N_+$ ,  $N_-$  as a function of the measured local slope  $\tan(\theta)$ [45] and applied load  $L$ , and of the unknown parameters  $\mu$  and  $c$ :

$$\begin{aligned} T_+ &= L \frac{\mu + \tan(\theta) + (c + \mu A)/(L \cos(\theta))}{1 - \mu \tan(\theta)} \\ N_+ &= L \cos(\theta) \frac{1 + \tan^2(\theta) + (c + \mu A) \tan(\theta)/(L \cos(\theta))}{1 - \mu \tan(\theta)} + A \\ T_- &= L \frac{\mu - \tan(\theta) + (c + \mu A)/(L \cos(\theta))}{1 + \mu \tan(\theta)} \\ N_- &= L \cos(\theta) \frac{1 + \tan^2(\theta) - (c + \mu A) \tan(\theta)/(L \cos(\theta))}{1 + \mu \tan(\theta)} + A \end{aligned} \quad (11)$$

Substituting Eqs. 11 into Eqs. 5, we obtain a set of equations from whom we aim to extract the values of the friction coefficient  $\mu$  and the offset  $c$ :

$$W = L\mu \frac{1 + \tan^2(\theta)}{1 - \mu^2 \tan^2(\theta)} + \frac{(c + \mu A)/\cos(\theta)}{1 - \mu^2 \tan^2(\theta)} \quad (12)$$

$$\Delta = T_{instr}(L) + \frac{L \tan(\theta)(1 + \mu^2)}{1 - \mu^2 \tan^2(\theta)} + \frac{\mu(c + \mu A) \tan(\theta)/\cos(\theta)}{1 - \mu^2 \tan^2(\theta)} \quad (13)$$

Here we have three unknown ( $T_{instr}$ ,  $\mu$  and  $c$ ) and only two equations. We may exploit the linearity of Eq. 12 in the applied load, in the form:

$$W \equiv \mu_{app}L + c_{app} \quad (14)$$

to extract the slope and the offset, both depending on the unknown  $\mu$  and  $c$ . The effect of a local tilt of the surface is the introduction of an apparent friction coefficient  $\mu_{app}$  and an apparent friction offset  $c_{app}$ :

$$\mu_{app}(\mu, \theta) = \mu \frac{1 + \tan^2(\theta)}{1 - \mu^2 \tan^2(\theta)} \quad (15)$$

$$c_{app}(\mu, c, \theta, A) = \frac{(c + \mu A)/\cos(\theta)}{1 - \mu^2 \tan^2(\theta)} \quad (16)$$

The linearity of Eq. 14 is a necessary condition for the validity of the assumption of the modified Amonton's law (only a necessary, and not sufficient condition !). Notice that, because of the dependence of  $T_{instr}$  on load  $L$ , we can not exploit Eq. 13 to extract the true values of  $\mu$  and  $c$  as for Eq. 12.

In the last equation we have explicitly indicated the dependence of  $T_{instr}$  on the load  $L$ . If the derivative of  $\Delta$  with respect to  $L$  is computed, as in the calibration procedure for the lateral sensitivity  $\alpha$  described by Ogletree *et al.* [24], the residual term  $dT_{instr}/dL$  can make the calibration procedure inaccurate (see discussion below).

Eq. 15 represents the well known topographic correction proposed by Bushan *et al.* [12] It is a 2nd-order equation whose meaningful root is the true friction coefficient  $\mu$ . This topographic correction holds under the assumptions that the friction is linearly dependent on the load and that the instrumental offset does not change in Trace and Retrace.

Because of the residual offset due to adhesion, the apparent friction coefficient  $\mu_{app}$  must be calculated via a fit of the  $W$  vs.  $L$  curve, and not simply as:  $\mu_{app} = W/L$ . This offset is present even in case a simple Coulomb-Amonton's law is assumed (i.e.  $c = 0$ ), and follows from considering explicitly the adhesion force in the decomposition of forces acting on the AFM tip (see Fig. 3). In the case of a flat surface ( $\theta = 0$ ) Eq. 18 reduces to the Amonton's-Coulomb equation:  $f = \mu(L + A)$ .

We end this section with some consideration about the application of the equations of the topographic corrections in the case of adhesive multi-asperity contact for the calculation of the cantilever lateral sensitivity  $\alpha$  proposed by Ogletree *et al.* in Ref. 24. Omitting the offset  $c$  in Eqs. 11-13, the following set of equations is obtained:

$$\begin{aligned}
T_+ &= L \frac{\mu + \tan(\theta)}{1 - \mu \tan(\theta)} + \frac{\mu A/L \cos(\theta)}{1 - \mu \tan(\theta)} \\
N_+ &= L \cos(\theta) \frac{1 + \tan^2(\theta)}{1 - \mu \tan(\theta)} + \frac{A}{1 - \mu \tan(\theta)} \\
T_- &= L \frac{\mu - \tan(\theta)}{1 + \mu \tan(\theta)} + \frac{\mu A/L \cos(\theta)}{1 - \mu \tan(\theta)} \\
N_- &= L \cos(\theta) \frac{1 + \tan^2(\theta)}{1 + \mu \tan(\theta)} + \frac{A}{1 + \mu \tan(\theta)}
\end{aligned} \tag{17}$$

and

$$W = L\mu \frac{1 + \tan^2(\theta)}{1 - \mu^2 \tan^2(\theta)} + \frac{\mu A/\cos(\theta)}{1 - \mu^2 \tan^2(\theta)} \tag{18}$$

$$\Delta = T_{instr}(L) + \frac{L \tan(\theta)(1 + \mu^2)}{1 - \mu^2 \tan^2(\theta)} + \frac{\mu^2 A \tan(\theta) / \cos(\theta)}{1 - \mu^2 \tan^2(\theta)} \quad (19)$$

Ogletree *et al.* obtained a set of equations slightly different from our Eqs. 18 and 19, because of the neglecting of adhesion  $A$  in the decomposition of forces along the normal direction. This however does not affect in principle the calculation of the lateral sensitivity  $\alpha$  because this is based on the *derivatives* of Eqs. 18 and 19 with respect to  $L$ . Derivation is supposed to clean off the offsets, as long as the dependence of  $T_{instr}$  on load  $L$  in Eq. 19 is weak. More precisely, in Eq. 19 the derivative of  $T_{instr}$  versus  $L$  must be (much) smaller than the term  $x = \tan(\theta)(1 + \mu^2)/(1 - \mu^2 \tan^2(\theta))$ . The procedure we have described in section III for the measurement of the instrumental offset, can be used to inquiry whether the method proposed by Ogletree *et al.* can be applied. If the derivative of  $T_{instr}$  versus  $L$  is comparable to  $x$ , the laser alignment should be optimized. This procedure should be followed each time a new cantilever is used, in order to validate the goodness of the laser alinement and minimize the unwanted effects of cross-talking. The main drawback of this procedure is that it requires a knowledge of both the tilt angle of the reference grating and the friction coefficient of the tip-grating pair.

## VI. EXPERIMENTAL SETUP AND DATA ANALYSIS

We have developed a complete quantitative protocol for the quantitative characterization of the friction properties of corrugated surfaces using the AFM, based on the equations derived so far.

We have used a Nanoscope Multimode IIIa AFM, that can be housed in a sealed chamber connected to a humidifier in order to work in controlled humidity and atmosphere (typically in dry and wet nitrogen). The deflection setpoint, determining the external applied load, is remotely controlled by a PC. The application of the load is synchronized with the end-line and end-frame triggers from the microscope, such that we can acquire a complete friction vs. load curve in a single AFM scan of typically 512 lines, 512 points per line. The experimental data are exported and post-processed via dedicated routines. Cantilever force constant  $k$  and lateral sensitivity  $\alpha$  are calibrated using the thermal noise method [37, 38, 39, 40] and the wedge method proposed by Ogletree *et al.* [24]. Our calibration methods do not require any analytical calculation based neither on the assumption of any oversimplified cantilever

geometry nor on SEM measurements, nor on any knowledge of the elastic properties of the cantilever material.

Our protocol requires the acquisition of four maps: the topographic map, the lateral force maps acquired in trace and retrace (i.e. the  $TR$  and  $RETR$  maps in volts) and the deflection setpoint map proportional to the external applied load  $L$ . These four maps should be recorded simultaneously because they are strictly in one-by-one correspondence. However, only up to two independent signals apart from the topographic one can be recorded simultaneously by our AFM controller. We record the topographic and lateral force maps together and the deflection setpoint map separately, because this is a quite stable and reproducible signal. We scan on the same line during one ramp, and repeat the ramp on different points. Adhesion is extracted from force versus distance curves acquired on a flat region of the sample. We repeat the adhesion measurement many times applying offsets in the  $xy$  directions and then averaging, in order to reduce the errors coming from the local corrugation of the surface. Assuming a constant adhesion across the whole scan window, an adhesion map  $A$  is readily obtained. Tip velocity is typically  $1 \mu m/s$ , scan size is up to  $1 \mu m$ , and resolution is 512 points per line. In each lateral force map we can change the applied load up to 512 times. Load range is typically 0-100 nN.

Topographic and lateral force maps are first smoothed using a one-dimensional kernel whose size equals the tip size (in point units), in order to smooth out all the information that are below the effective resolution limit. The map of local slopes  $\tan(\theta)$  is calculated from the topographic map, with a resolution equal to the tip radius  $R$ , so that we have  $\tan(\theta) \sim \tan(\theta)_R$  (see section II). At this point we calculate  $W$  from  $TR$  and  $RETR$  (Eq. 4). The map of local slopes, the map of external loads  $L$ , and the  $W$  map are in one-to-one correspondence. Making a sampling of the slope map and exploiting the one-to-one correspondence with other maps, the family of sets  $\{W, L\}_\theta$  is obtained, each containing the pairs  $\{W, L\}$  corresponding to points in the topographic map having the same slope. Each set gives a  $W$  vs.  $L$  characteristics (an example is shown in Fig. 5) that in turn can be fitted to extract the apparent friction coefficient  $\mu_{app}(\mu, \theta)$  and the apparent adhesive offset  $c_{app}(\mu, c, \theta, A)$ . The linear fit is weighted with errors on both  $W$  and  $L$  coming from the indetermination on the vertical force constant  $k$ ,  $z$ -sensitivity  $z-sens$ , and lateral sensitivity  $\alpha$  (see Appendix ). From the apparent friction coefficient  $\mu_{app}$ , given the slope  $\tan(\theta)$ , the true friction coefficient  $\mu$  is extracted (Eq. 15). From the apparent adhesive offset  $c_{app}$ , given

the slope, the adhesion map, and the friction coefficient  $\mu$ , the adhesive offset  $c$  is extracted (Eq. 16). The propagation of errors is taken into account in order to determine the error on both  $\mu$  and  $c$  (Eqs. A.7 and A.12). The errors calculated for  $\mu$  and  $c$  are in turn used to obtain the weighted distributions of measured values of  $\mu$  and  $c$  (Fig. 6). Finally, average values and standard deviations are obtained fitting the histograms with gaussian curves.

## VII. RESULTS AND DISCUSSION

In order to illustrate the importance of the topographic correction for the measurement of the friction coefficient of corrugated surfaces with FFM, we compare the lateral force dispersion measured by FFM on a Polytetrafluoroethylene (PTFE) sample with the theoretical predictions of Eq. 12, evaluated using the measured values of the friction coefficient and adhesive offsets.

The dispersion of the measured lateral force values is shown in Fig. 7. The friction coefficient and the adhesive offset, as measured with the topographic correction procedure, are  $\mu = 0.057 \pm 0.009$  and  $c = 0.81 \pm 0.17$  nN. Other parameters are:  $\alpha = 30$  nN/V,  $k = 0.1$  N/m,  $z_{sens} = 116$  nm/V and adhesion  $A = 7$  nN. The lateral force dispersion of the PTFE corrugated sample simulated using Eq. 12 is shown in Fig. 8 (the distribution of tilt angles of the PTFE sample is shown in the inset, together with a topographic profile). The effect of the presence of a distribution of tilt angles at the sample surface is the coexistence in Fig. 8 of several linear trends, one stronger (corresponding to the intense peaks in the tilt angle distribution between -10 and -20 degs) and the others wicker. In the experimental dispersion we find qualitatively the same trend, although the statistical noise makes the different linear trends mixing and broadening. The topographic correction would make all the linear trends collapse into one. Neglecting the topographic correction would likely lead to inaccurate measurements of the friction coefficient. In order to quantify the error induced by the presence of a distribution of tilt angles at the sample surface, we plot in Fig. 9 the relative error  $(\mu_{app} - \mu)/\mu$ , calculated from Eq. 15, versus the tilt angle. In the calculation of  $(\mu_{app} - \mu)/\mu$  we assumed  $\mu = 0.05$ , although the result is largely independent on the value of  $\mu$ . It can be noticed that for tilt angles bigger than about 20 degs the discrepancy increases rapidly above 10% and becomes larger than 70% at 40 degs. The slopes in the region of the leading trends in Fig. 7 span approximately from 0.056 to 0.061. The difference is of



the order of 10%, which is the expected deviation induced by tilt angles below 20 degrees. The topographic correction is required as long as the mean tilt is larger than about 15-20 degrees.

The presence of a distribution of tilt angles amplifies the statistical noise on the measured values of the lateral force. In addition, it must be considered that often additional trends are present in the lateral force map, due to those contributions to friction which are not accounted for by the topographic correction, such as the ploughing and the collision effect [12], etc... Even in the case of small tilt angles, the topographic correction procedure can help in minimizing the effects of this noise.

The validity of the friction model that we have adopted in the topographic correction procedure can be verified a posteriori from the linearity of the experimental  $W$  vs.  $L$  curves and from the values of the adhesive offset  $c$ . We have found that the modified Amonton's law is appropriate in describing the frictional behaviour of a number of systems in ambient conditions (nanostructured carbon films grown via Supersonic Cluster Beam Deposition [41], PTFE-based coatings obtained through syntherization of nanoemulsions [42], and silicon) , for loads below 100 nN. The measured values of the adhesive offset  $c$  were always different from zero, in the limit of the experimental error. Typical values of the adhesive offset measured are up to few nanonewtons. If this offset was due to a mere uncertainty in the measurement of the adhesion force, we should assume a relative error in its measurement larger than 100%. For smaller values of  $c$ , well below 1 nN, relative errors in  $A$  of the order 20-40% could in fact be compatible with the simple Coulomb equation (see Eq. 9). However, if the adhesion force is carefully extracted averaging over many force vs. distance curves, we believe that the error associated can be of the order of 10%. We are thus confident that our experimental data support the validity of the modified Amonton's law as an effective friction model, whose origin must be deeply investigated in the framework of adhesive contact mechanics. We finally notice that if wear takes place during scanning, the tip-sample interface and, consequently, the adhesion force would change. This would represent an additional source of noise, in that the value of adhesion used in the fit would not correspond to the actual ones. This effect can be minimized, if not avoided, operating the microscope in the low-load regime.

We point out finally that the relative errors in the measured friction coefficients and adhesive offsets are typically comparable with that of the factor  $z_{sens} \cdot k/\alpha$ , which basically

convert the friction coefficient extracted from the experimental data in Volts into the true one. This error is typically 15-30%, depending on the accuracy of the cantilever calibration procedures. This error can be considered systematic and can be reduced only improving the accuracy of the calibration methods (and this is actually one of the bottlenecks of nano-friction measurements). The statistical errors in the measured lateral force values are instead efficiently smoothed out by our protocol, because of the large number of points that are processed in a single image, the large number of lateral force maps that can be acquired in a reasonable time.

## VIII. CONCLUSIONS

We have discussed the problem of the topographic correction of lateral force maps, which is necessary to obtain quantitative information on the tribological properties of corrugated samples via FFM experiments. We have recognized that there are intrinsic instrumental limitations which reduce the accuracy of these measurements. In particular, the unreliable measurement of the instrumental lateral force offset poses severe limitations to the applicability of the topographic correction and should be taken into account whenever the decomposition of forces on a locally tilted surface is considered, such as in the procedure for the calibration of the lateral sensitivity proposed in Ref. 24.

Assuming that the friction behavior is well described by a modified Amonton's law, where a constant offset is explicitly considered in order to account for the zero-load friction force typical of single asperity adhesive friction, we have solved the problem of the topographic correction of FFM lateral force maps and developed a complete protocol, which provide quantitative and reliable characterization of frictional properties of corrugated materials. The final error in the measurement is basically due to the uncertainty in the force constants of the cantilever and it is typically of the order of 15-30%. Neglecting the topographic correction on corrugated samples can lead to even larger errors.

The frictional model adopted is appropriate to describe the behavior of many systems in humid environment. The quantitative assessment of this offset is important in order to determine the total friction force, for comparison among different materials.

## APPENDIX: ERROR ANALYSIS

We extract an apparent friction coefficient  $\mu_{app}$  and an apparent offset  $c_{app}$  via a linear fit of the  $W$  vs.  $L$  curve (Eq. 12). Notice that the original signals  $W$  and  $L$ , as well as the adhesion force  $A$ , are given in Volts. They must be converted in nanoNewton using the cantilever vertical force constant  $k$  in  $N/m$  and sensitivity  $z-sens$  in  $nm/V$ , and the lateral sensitivity  $\alpha$  in  $nN/V$ . We assume a relative error of 10% for  $k$  and  $\alpha$  and of 2% for  $z-sens$ , which is calculated from the slope of force-vs.-distance curves taken on a hard flat surface, averaging over many acquisitions. The relative error for the applied load  $L$  is thus 12%, that for the lateral force  $W$  is 10%. The linear fit of the  $W$  vs.  $L$  curve is weighted with the errors of  $W$  and  $L$ . We use the error of  $A$  later in the error propagation analysis. Notice that the relative error associated to adhesion (15%) comes from the force constant (10%) and from the statistical error associated to the extraction of the adhesion force from many force vs. distance curves (5%). The error in  $z-sens$  does not contribute to the error of  $A$  because the depth of the pull-off region in the approaching-retracting curve is calculated on the retraction length axis directly in nm with good accuracy.  $\mu$  and  $c$  are the true incognitae of the problem, while  $A$ ,  $\theta$ ,  $W$  and  $L$  are known or measured, each with its own error. From Eqs. 15 and 16 we have:

$$\mu(\mu_{app}, \theta) = \frac{-\frac{1+\tan^2(\theta)}{\mu_{app}} + \sqrt{\left(\frac{1+\tan^2(\theta)}{\mu_{app}}\right)^2 + 4 \tan^2(\theta)}}{2 \tan^2(\theta)} \quad (\text{A.1})$$

$$c(\mu, c_{app}, \theta, A) = c_{app} \cos(\theta)(1 - \mu^2 \tan^2(\theta)) - \mu A \quad (\text{A.2})$$

We apply standard error propagation analysis to Eqs. A.1 and A.2 to calculate the errors of  $\mu$  and  $c$  (the error in  $\theta$  is negligible):

$$\delta\mu^2 = \left(\frac{\delta\mu}{\delta\mu_{app}}\right)^2 \delta\mu_{app}^2 \quad (\text{A.3})$$

$$\delta c^2 = \left(\frac{\delta c}{\delta\mu}\right)^2 \delta\mu^2 + \left(\frac{\delta c}{\delta c_{app}}\right)^2 \delta c_{app}^2 + \left(\frac{\delta c}{\delta A}\right)^2 \delta A^2 \quad (\text{A.4})$$

We calculate first  $\frac{\delta\mu}{\delta\mu_{app}}$ :

$$\begin{aligned} \frac{\delta\mu}{\delta\mu_{app}} &= \frac{1}{2 \tan^2(\theta)} \left\{ \frac{1 + \tan^2(\theta)}{\mu_{app}^2} - \left[ \left( \frac{1 + \tan^2(\theta)}{\mu_{app}} \right)^2 + 4 \tan^2(\theta) \right]^{-1/2} \left( \frac{1 + \tan^2(\theta)}{\mu_{app}^3} \right) \right\} \\ &= \frac{1}{2 \tan^2(\theta)} \left( \frac{1 + \tan^2(\theta)}{\mu_{app}^2} \right) \left\{ 1 - \frac{1 + \tan^2(\theta)}{\mu_{app}} \left[ \left( \frac{1 + \tan^2(\theta)}{\mu_{app}} \right)^2 + 4 \tan^2(\theta) \right]^{-1/2} \right\} \\ &= \frac{1}{2 \mu_{app} \tan(\theta)} \frac{1 + \tan^2(\theta)}{\mu_{app} \tan(\theta)} \left\{ 1 - \frac{1 + \tan^2(\theta)}{\mu_{app} \tan(\theta)} \left[ \left( \frac{1 + \tan^2(\theta)}{\mu_{app} \tan(\theta)} \right)^2 + 4 \right]^{-1/2} \right\} \end{aligned}$$

Setting

$$x = \frac{1 + \tan^2(\theta)}{\mu_{app} \tan(\theta)} \quad (\text{A.5})$$

we obtain:

$$\frac{\delta\mu}{\delta\mu_{app}} = \frac{x}{2\mu_{app} \tan(\theta)} [1 - x(x^2 + 4)^{-1/2}] \quad (\text{A.6})$$

and from Eq. A.3:

$$\delta\mu^2 = \left(\frac{x}{2\mu_{app} \tan(\theta)}\right)^2 [1 - x(x^2 + 4)^{-1/2}]^2 \delta\mu_{app}^2 \quad (\text{A.7})$$

Because  $x^2 \gg 4$ , Eq. A.7 can be replaced with:

$$\delta\mu^2 = \left(\frac{1}{1 + \tan^2(\theta)}\right)^2 \delta\mu_{app}^2 \quad (\text{A.8})$$

Concerning the error  $\delta c^2$ , we have:

$$\frac{\delta c}{\delta\mu} = -(A + 2c_{app} \cos(\theta) \tan^2(\theta)\mu) \quad (\text{A.9})$$

$$\frac{\delta c}{\delta c_{app}} = \cos(\theta)(1 - \mu^2 \tan^2(\theta)) \quad (\text{A.10})$$

$$\frac{\delta c}{\delta A} = -\mu \quad (\text{A.11})$$

and finally:

$$\delta c^2 = \cos^2(\theta)(1 - \mu^2 \tan^2(\theta))^2 \delta c_{app}^2 + (A + 2c_{app} \cos(\theta) \tan^2(\theta)\mu)^2 \delta\mu^2 + \mu^2 \delta A^2 \quad (\text{A.12})$$

## ACKNOWLEDGMENTS

The authors would like to thank M. Coletti for its contributions in the development of the nanotribological protocol.

- 
- [1] *Materials Research Society Bulletin*, vol. 26 (2001).
  - [2] B. Bhushan, *Handbook of Micro and Nano Tribology* (CRC Press, 1999).
  - [3] B. Bhushan, *Proc. Instn. Mech. Engrs* **215** (2001).
  - [4] R. Carpick and M. Salmeron, *Chem. Rev.* **97**, 1163 (1997).
  - [5] G. Dedkov, *Phys. Stat. Sol. (a)* **179**, 3 (2000).
  - [6] E. Gnecco, R. Bennewitz, T. Gyalog, and E. Meyer, *J. Phys.: Cond. Matt.* **13**, R619 (2001).

- [7] G. Meyer and N. Amer, *Appl. Phys. Lett.* **57**, 2089 (1990).
- [8] S. Grafstrom, M. Neitzert, T. Hagen, J. Ackermann, R. Neumann, O. Probst, and M. Wortge, *Nanotechnology* **4**, 143 (1993).
- [9] M. Labardi, M. Allegrini, and F. Fuso, *J. Vac. Sci. Technol.* **B12**, 1642 (1994).
- [10] M. Labardi, M. Allegrini, M. Salerno, C. Frediani, and C. Ascoli, *Appl. Phys. A* **59**, 3 (1994).
- [11] V. Koinkar and B. Bhushan, *J. Appl. Phys.* **81**, 2472 (1997).
- [12] S. Sundararajan and B. Bushan, *J. Appl. Phys.* **88**, 4825 (2000).
- [13] R. Carpick, N. Agrait, D. Ogletree, and M. Salmeron, *J. Vac. Sci. Tech.* **B14**, 1289 (1996).
- [14] U. Schwarz, W. Allers, G. Gensterblum, and R. Wiesendanger, *Phys. Rev. B* **52**, 14976 (1995).
- [15] M. Enachescu, R. van den Oetelaar, R. Carpick, D. Ogletree, C. Flipse, and M. Salmeron, *Phys. Rev. Lett.* **81**, 1877 (1998).
- [16] R. Bennewitz, E. Gnecco, T. Gyalog, and E. Meyer, *Tribology Letters* **10**, 51 (2001).
- [17] F. Bowden and D. Tabor, *The Friction and Lubrication of Solids* (Clarendon, Oxford, 1950).
- [18] B. Bhushan, ed., *Fundamentals of Tribology and Bridging the Gap between Macro- and Micro/Nanoscales*, vol. 10 of *NATO ASI Series* (Kluwer Academic Publishers, 2001).
- [19] B. Bhushan, *Modern Tribology Handbook*, vol. 1 (CRC Press, 2001).
- [20] A.-L. Barabasi and H. E. Stanley, *Fractal Concepts in Surface Growth* (University Press, Cambridge, 1995).
- [21] G. Adams and M. Nosonovsky, *J. Trib.* **33**, 431 (2000).
- [22] U. Schwarz, O. Zworner, P. Koster, and R. Wiesendanger, *Phys. Rev. B* **56**, 6987 (1997).
- [23] J.-A. Ruan and B. Bhushan, *J. Trib.* **116**, 378 (1994).
- [24] D. Ogletree, R. Carpick, and M. Salmeron, *Rev. Sci. Instr.* **67**, 3298 (1996).
- [25] J. Israelachvili, *Intermolecular and surface forces* (Academic Press, 1992).
- [26] M. Lantz, S. O'Shea, and M. Welland, *Phys. Rev. B* **56**, 15345 (1997).
- [27] P. Frantz, A. Artsyukhovich, R. Carpick, and M. Salmeron, *Langmuir* **13**, 5957 (1997).
- [28] C. Putman and M. Igarashi, *Appl. Phys. Lett.* **66**, 1 (1995).
- [29] K. Fuller and D. Tabor, *Proc. R. Soc. Lond. A* **345**, 327 (1975).
- [30] A. Bush, R. Gibson, and G. Keogh, *Mechanics Research Communications* **3**, 169 (1976).
- [31] K. Kendall, *Science* **319**, 203 (1986).
- [32] B. Persson and E. Tosatti, *Journal of Chemical Physics* **115** (2001).
- [33] T. Chow, *Phys. Rev. Lett.* **86**, 4592 (2001).

- [34] K. Johnson, K. Kendall, and A. Roberts, Proc. R. Soc. Lond. **A324**, 301 (1971).
- [35] B. Derjaguin, V. Muller, and Y. P. Toporov, J. Coll. Int. Sci. **53**, 314 (1971).
- [36] U. Schwarz, H. Bluhm, H. Holscher, W. Allers, and R. Wiesendanger, in *Physics of sliding friction*, edited by B. Persson and E. Tosatti (Kluwer Academic Publishers, Netherlands, 1996), p. 369.
- [37] H.-J. Butt and M. Jaschke, Nanotechnology **6**, 1 (1995).
- [38] J. Sader, J. Appl. Phys. **84**, 64 (1998).
- [39] R. Stark, T. Drobek, and W. Heckl, Ultramicroscopy **86**, 207 (2000).
- [40] R. Levy and M. Maaloum, Nanotechnology **13**, 33 (2002).
- [41] A. Podestà, G. Fantoni, P. Milani, M. Ragazzi, D. Donadio, and L. Colombo, J. Nanosci. Nanotechnol. (2002).
- [42] A. Podestà, G. Fantoni, P. Milani, C. Guida, and S. Volponi, Thin Solid Films **419**, 154 (2002).
- [43] Notice that  $\mathbf{L}$  is the *externally* applied load, as measured from the deflection of the cantilever, controlled by the deflection setpoint.
- [44] The instrumental offset cancels out under the hypothesis that it does not change in Trace and Retrace.
- [45] Hereafter we assume  $\tan(\theta) \equiv \tan(\theta)_R$ , where  $R$  is the tip radius (see section II).

## FIGURE CAPTIONS

Figure 1. Experimental friction loop. The measured  $TR$  and  $RETR$  signals and their half-sum  $\Delta$  and half-difference  $W$  are shown.

Figure 2. Schematic representation of the contact between the AFM tip and the sample surface, characterized by the correlation length  $\xi$ . The cases  $\xi/R \leq 1$  (left) and  $\xi/R \geq 1$  (right) are shown. The tilt of the surface calculated with resolution equal to the radius of the bigger probe,  $\theta^*$ , is also shown.

Figure 3. Forces diagram for the AFM tip sliding down a sloped topographic feature (retrace).

Figure 4. The instrumental offset  $T_{instr}$  as a function of the external applied load.

Figure 5.  $\{W, L\}_\theta$  characteristics.

Figure 6. Weighted histograms of values of  $\mu$  and  $c$  extracted from each  $\{W, L\}_\theta$  characteristics.

Figure 7. Dispersion of lateral force values measured on the PTFE sample without the topographic correction.

Figure 8. Lateral force dispersion of a PTFE sample simulated from Eq. 12 using topographic and frictional parameters as given by the friction analysis. In the inset are shown the topographic profile and the slope distribution of the PTFE sample whose lateral force distribution is shown in Fig. 7.

Figure 9. Relative error in the measured friction coefficient as a function of the local tilt angle  $\theta$ .

## FIGURES



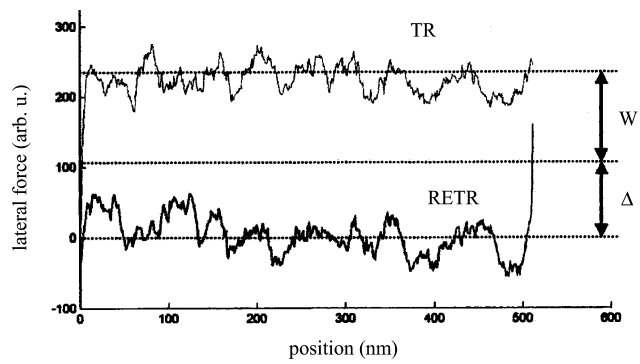


FIG. 1:

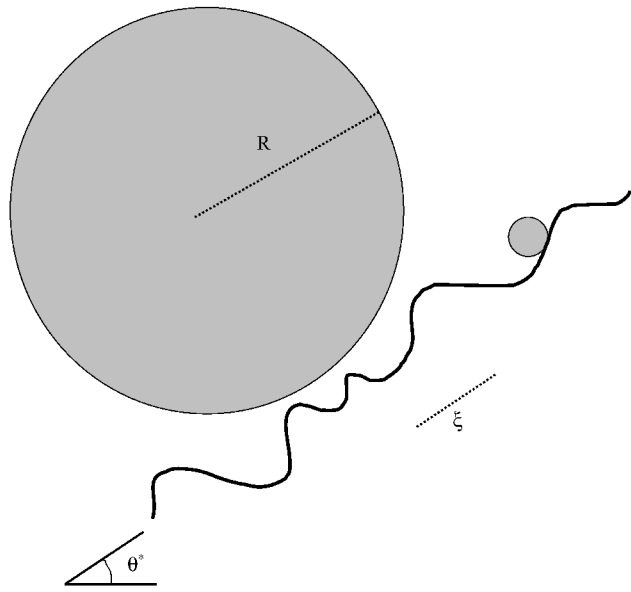


FIG. 2:

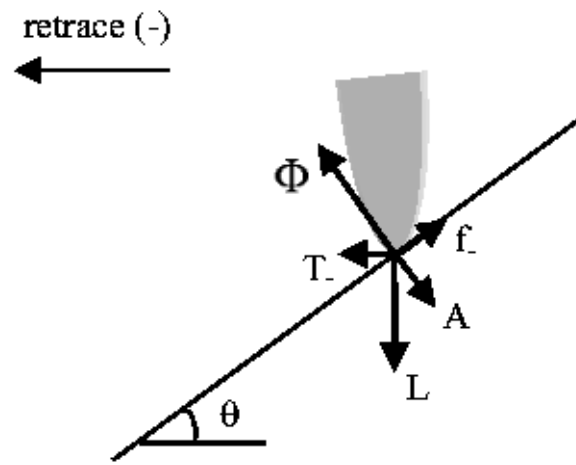


FIG. 3:

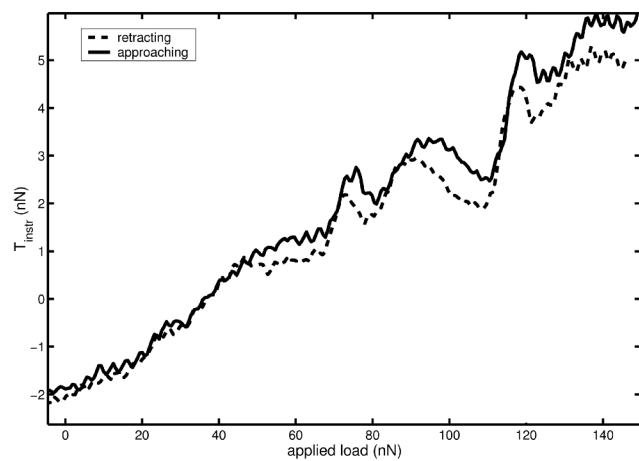


FIG. 4:

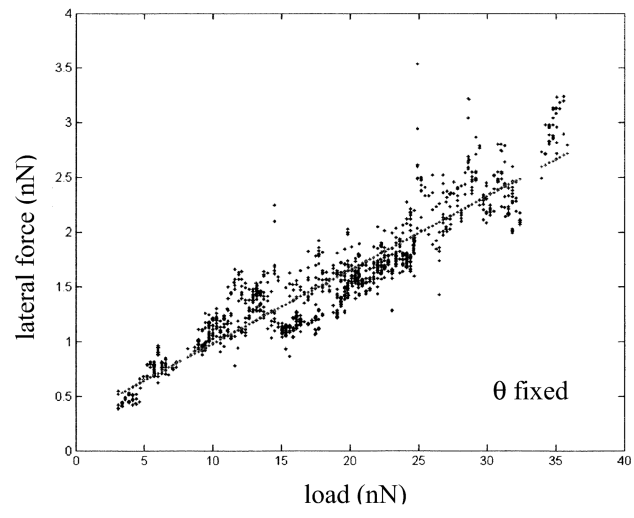


FIG. 5:

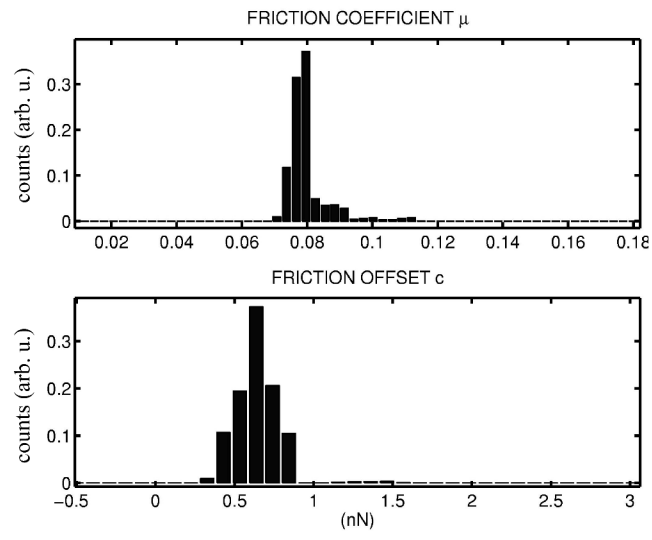


FIG. 6:

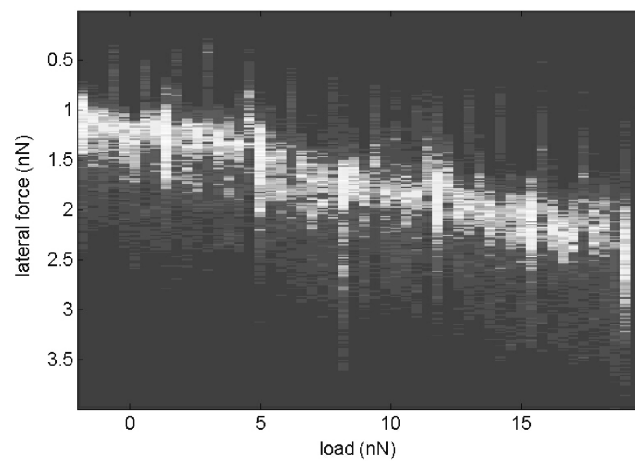


FIG. 7:

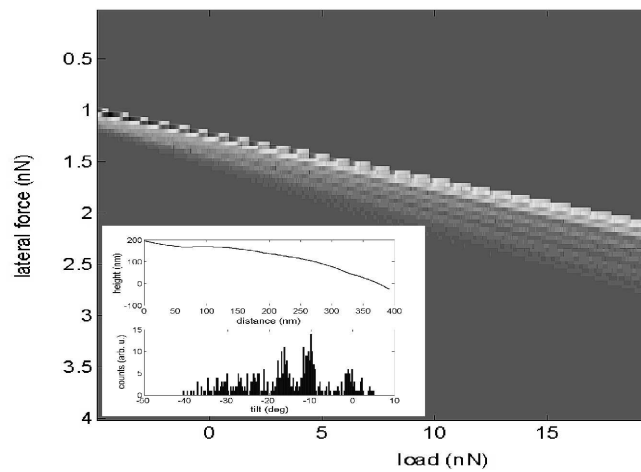


FIG. 8:



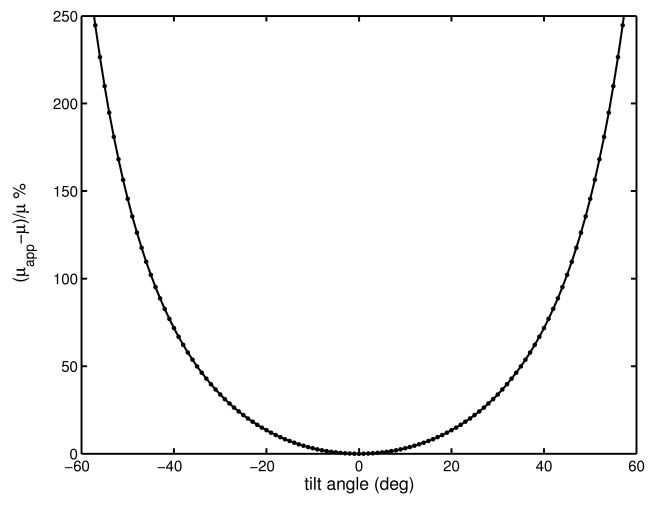


FIG. 9: